Proteomic and lipidomic analyses of the Arabidopsis atg5 autophagy mutant reveal major changes in endoplasmic reticulum and peroxisome metabolisms and in lipid composition

Marien Havé, Jie Luo, Frédérique Tellier, Thierry Balliau, Gwendal Cueff, Fabien Chardon, Michel Zivy, Loïc Rajjou, Jean-Luc Cacas, Céline Masclaux-daubresse

Proteomic and lipidomic analyses of the Arabidopsis *atg5* autophagy mutant reveal major changes in endoplasmic reticulum and peroxisome metabolisms and in lipid composition

Marien Havé[1]*, Jie Luo[1]*, Frédérique Tellier[1], Thierry Balliau[2], Gwendal Cueff[1], Fabien Chardon[1], Michel Zivy[2], Loic Rajjou[1], Jean-Luc Cacas[1] and Céline Masclaux-Daubresse[1]

[1]Institut Jean-Pierre Bourgin, INRA, AgroParisTech, CNRS, Université Paris-Saclay, 78000 Versailles, France; [2]UMR GQE- le Moulon, INRA, Université Paris-Sud, CNRS, AgroParisTech, Université Paris-Saclay, 91190Gif-sur-Yvette, France

Author for correspondence:
Céline Masclaux-Daubresse
Tel: +33 1 30 83 30 88
Email: celine.masclaux-daubresse@inra.fr

Received: *5 February 2019*
Accepted: *29 April 2019*

New Phytologist (2019) **223:** 1461–1477
doi: 10.1111/nph.15913

Key words: endomembrane, endoplasmic reticulum stress, lipids, nitrate limitation, plant metabolism, salicylic acid (SA), sulfur limitation, β-oxidation.

Summary

- Autophagy is a universal mechanism in eukaryotic cells that facilitates the degradation of unwanted cell constituents and is essential for cell homeostasis and nutrient recycling.
- The salicylic acid-independent effects of autophagy defects on leaf metabolism were determined through large-scale proteomic and lipidomic analyses of *atg5* and *atg5/sid2* mutants under different nitrogen and sulfur growth conditions.
- Results revealed that irrespective of the growth conditions, plants carrying the *atg5* mutation presented all the characteristics of endoplasmic reticulum (ER) stress. Increases in peroxisome and ER proteins involved in very long chain fatty acid synthesis and β-oxidation indicated strong modifications of lipid metabolism. Lipidomic analyses revealed changes in the concentrations of sphingolipids, phospholipids and galactolipids. Significant accumulations of phospholipids and ceramides and changes in GIPCs (glycosyl-inositol-phosphoryl-ceramides) in *atg5* mutants indicated large modifications in endomembrane-lipid and especially plasma membrane-lipid composition. Decreases in chloroplast proteins and galactolipids in *atg5* under low nutrient conditions, indicated that chloroplasts were used as lipid reservoirs for β-oxidation in *atg5* mutants.
- In conclusion, this report demonstrates the strong impact of autophagy defect on ER stress and reveals the role of autophagy in the control of plant lipid metabolism and catabolism, influencing both lipid homeostasis and endomembrane composition.

Introduction

Autophagy (meaning self-eating) is a universal mechanism in eukaryotic cells that facilitates the degradation of unwanted cell constituents. Macro-autophagy (from this point referred to as autophagy) consists of the formation of double membrane vesicles termed autophagosomes, located in the cytosol, and that engulf and sequester unwanted cytoplasmic constituents such as damaged organelles and protein aggregates (Liu & Bassham, 2012). In plants, autophagosomes drive their cargoes to the lytic vacuole where proteases and hydrolases degrade them. As cargoes are not only proteins but also organelles, autophagy is also involved in the recycling of membranes and of micronutrients (Masclaux-Daubresse *et al.*, 2017; Pottier *et al.*, 2019).

Autophagosome formation requires the products of 18 AUTOPHAGY (*ATG*) genes that constitute the core machinery of autophagy (Yang & Bassham, 2015). Among these, *ATG5* is involved in the ATG5−ATG12 conjugation system which is essential for the formation of the ATG8−PE (PE, phosphatidylethanolamine) conjugate. ATG8−PE that forms part of the autophagosome membrane is needed for the expansion of the vesicle and to bind autophagy receptors and cargoes (Masclaux-Daubresse *et al.*, 2017).

The 'omics studies performed on autophagy mutants by different research groups have highlighted several metabolic disturbances under standard growth conditions and under various nutrient starvations. They provided several lines of evidence that autophagy plays an important role in plant adaptation to stresses (Liu *et al.*, 2018 for a review). Dysregulations of sugar, amino acid and lipid contents were investigated (Izumi *et al.*, 2013b; Kurusu *et al.*, 2014; Masclaux-Daubresse *et al.*, 2014; Avin-Wittenberg *et al.*, 2015; McLoughlin *et al.*, 2018). The transcriptomic study performed by Masclaux-Daubresse *et al.* (2014) showed that genes involved in salicylic acid (SA) and ethylene biosynthesis were upregulated in *atg5* and *atg9* compared with wild-type. This was consistent with the increased levels of SA and ethylene found in atg mutants. The expression of the master genes involved in the flavonoid pathway was downregulated, in

*These authors contributed equally to this work.

good agreement with the lower flavonoid content in atg5 and atg9. Several WRKY and NAC (no apical meristem (NAM), *Arabidopsis thaliana* transcription activation factor (ATAF1/2) and cup-shaped cotyledon (CUC2)) transcription factors involved in stress responses or senescence were significantly increased. The transcriptomic analyses performed further on the transgenic Arabidopsis lines overexpressing *ATG5* or *ATG7* confirmed these outcomes, showing that many genes involved in SA signaling, proteolysis and lipid degradation were downregulated, while transcripts involved in flavonoid and anthocyanin biosynthesis were upregulated in overexpressors (Minina *et al.*, 2018).

The multiomic study performed on maize *atg12* mutant by McLoughlin *et al.* (2018), confirmed many of the metabolic features found in Arabidopsis. From proteome/transcriptome comparisons, authors established the role of autophagy in clearing peroxisomes, Golgi bodies, ER, ribosomes and proteasome, and found possible role of autophagy in regulating fatty acid catabolism (McLoughlin *et al.*, 2018).

The *atg5* Arabidopsis mutant largely used in several studies on plant autophagy (Havé *et al.*, 2018 and reference therein) is strongly impaired in N remobilisation (Guiboileau *et al.*, 2012). It displays higher protein concentrations than wild-type in its leaves and contains higher endo-, carboxy- and amino-peptidase activities (Guiboileau *et al.*, 2013). It seems that in the absence of autophagosome trafficking, proteases and their substrates could not meet, resulting in the overaccumulation of nondegraded proteins. The presence in large abundance of uncomplete degradation products may in turn stimulate protease activities. Using global and activity-based proteomic analyses, Havé *et al.* (2018) identified the nature of the overabundant proteases in autophagy mutants. They showed that most of these are well known cysteine proteases. They also showed that proteasome activity was increased in the *atg5* mutants.

The aim of this study was to use proteomics to explore protein abundances in *atg5*, to clarify how autophagy influences cell physiology and metabolism. Because part of the phenotypes of *atg5* is due to the higher concentration of SA in its leaves, we compared *atg5* vs Col and *atg5/sid2* vs *sid2* to identify the SA-independent effects of the mutation. Three different nitrogen and sulfur supplies were used to identify changes that were unrelated to nutrient availabilities. Together with the liquid chromatography−mass spectrometry (LC−MS) lipidomic analyses performed on *atg5* mutants, proteomic results provide a comprehensive picture of how autophagy influence lipid metabolism and homeostasis in Arabidopsis, independently of N or S limitations.

Materials and Methods

Plant material and growth conditions

Arabidopsis thaliana (L.) Columbia wild-type, *atg5* mutant (*atg5-3*, SALK_020601), *sid2* (*sid2-2*; Dewdney *et al.*, 2000) and *atg5/sid2* double mutant have been previously characterised by Yoshimoto *et al.* (2009). Plants were cultivated according to Havé *et al.* (2018), under control conditions (Ctr; 10 mM NO_3^- and 0.266 mM SO_4^{2-}), low nitrate (LN; 2 mM NO_3^- and 0.266 mM SO_4^{2-}) or low sulfur (10 mM NO_3^- and 0.016 mM SO_4^{2-}) conditions. For control and low-S conditions each pot contained one plant; under low-N conditions there was six plants per pot. Details on these adequate growth conditions for trial of nitrogen limitation effects on Arabidopsis are explained in Havé *et al.* (2018). Whole rosettes were harvested 60 d after sowing (DAS). Four biological replicates were obtained. For control and low-S conditions, biological replicates contained the rosettes of four plants. For low-N conditions, biological replicates contained 24 rosettes. Harvests were performed between 10:00 and 11:00 h, and samples were stored at −80°C for further experiments. Plant culture was repeated three times, providing samples from three independent experiments.

Shotgun proteomic analysis

Extraction of total leaf proteins, trypsin digestion, LC−MS/MS analyses and protein identification were performed according to Havé *et al.*, 2018, at the PAPSSO platform (INRA, Le Moulon, Gif-sur-Yvette). Peptide quantification by peak area integration on eXtracted ion chromatogram (XICs) was performed using the MassChroQ software (pappso.inra.fr/bioinfo/masschroq/) according to Balliau *et al.* (2018). Normalisation was performed considering peptide retention time as described in Lyutvinskiy *et al.* (2013). Proteins were quantified based on peptide intensities by filtering for protein-specific peptides present in at least 90% of the samples and showing a significant correlation ($r > 0.6$) with the other peptides of the same protein. Relative protein abundances were then calculated and defined as the sum of XICs intensities of selected peptides. When peptides of a protein were not present or not reproducibly observed in one or several conditions, spectral counting (SC) was used in place of XICs analysis. Only proteins that produced at least four protein-specific spectra in at least one sample were considered for SC quantification. We considered that proteins which did not match this threshold were of too low an abundance to be reliably quantified.

Transcriptomic data

Transcriptomic data used to determine changes between autophagy mutants and control lines were obtained from Masclaux-Daubresse *et al.* (2014) and from microarray analyses performed at 'Plateforme Biopuces et Séquençage' (IGBMC, Strasbourg, France) using the Affymetrix ATH1 microarrays according to manufacturer's instructions.

Bioinformatics and statistical analysis

All statistical analyses were performed using the R software (https://www.R-project.org/).

Proteomic data were analysed using Tukey test in R, comparing *atg5* and *atg5/sid2* vs Col and *sid2*, respectively, in each growth conditions. Among the proteins with significant change in abundance (P-value < 0.05), only those with fold change (FC) higher than 1.2 were further considered. For transcriptome analyses, raw data were normalised and computed in R software

(https://www.R-project.org/) with LIMMA package. Empirical BAYES statistics within LIMMA package was used to compute t-statistic of differential expression, *P*-values of *t*-tests were corrected by Benjamini–Hochberg multiple testing (Benjamini & Hochberg, 1995). Significant genes in the comparisons of *atg5* vs Col and *atg5/sid2* vs *sid2* under each condition were selected using FC > 2 with FDR < 0.05 as threshold. Functional information and cellular location for each protein were analysed using VIRTUALPLANT 1.3 (http://virtualplant.bio.nyu.edu/cgi-bin/vpweb/), MAPMAN (https://mapman.gabipd.org/) databases and SUBA4 (http://suba.live/). Gene Ontology and KEGG analyses were conducted in R with the CLUSTERPROFILER and PATHVIEW packages (Yu *et al.*, 2012; Luo & Brouwer, 2013).

Lipid extraction and analyses

Total fatty acids, originating from all the lipids present in the cell, were measured after fatty acids methyl ester (FAME) preparation from 2 mg of material followed by gas chromatography–mass spectrometry (GC)-MS analysis according to Li *et al.* (2006). Phospholipids, galactolipids and shingolipids were extracted from plant material as described previously (Tellier *et al.*, 2014). Here, 1 ml of extraction solvent (isopropanol : hexane : water, 55 : 20 : 25) and 10 µl of adequate internal standards were added to 2 mg of grinded and freeze-dried material and the sample was incubated at 60°C for 15 min. Sphingolipid and phospholipid standards were purchased from AvantiPolar Lipids Inc. (Alabaster, AL, USA) and galactolipid standards from Matreya LLC (State College, PA, USA). The standards used for quantification of sphingolipids were GM1 (20 nmol), C12-GlcCer (10 nmol) and C12-Cer (1 nmol) in 1 ml of extraction solvent (isopropanol : hexane : water, 55 : 20 : 25). Those used for quantification of phospholipids and galactolipids were PC28:0 (10 nmol), PE31:1 (10 nmol), PI31:1 (10 nmol), PG28:0 (10 nmol), PS28:0 (1 nmol), PA28:0 (1 nmol), MGDG36:0 (10 nmol) and DGDG36:0 (10 nmol) in 1 ml of extraction solvent. After centrifugation at 1699 ***g*** for 5 min, the supernatant was recovered and the pellet extracted once more with 1 ml of extraction as previously. Supernatants were combined, dried with a Speed-Vac evaporator and stored at −20°C. To improve ionisation, the samples dedicated to sphingolipids analysis were subjected to alkaline hydrolysis. Samples were re-suspended by sonication in 100 µl of tetrahydrofuran (THF) : methanol : water (2 : 1 : 2) containing 0.1% formic acid (for GIPCs, GlcCers, phospholipids and galactolipids) or THF (for Cers and hCers) and filtrated before analysis. Ultra-high performance liquid chromatography (UPLC)–electrospray ionisation (ESI) –tandem mass spectrometry (MS/MS) analyses were carried out on a Waters Acquity UPLC system coupled to a Waters Xevo tandem quadrupole mass spectrometer (Manchester, UK) equipped with an ESI source. The mass analyses were performed in the positive or negative multiple reaction monitoring (MRM) mode. Chromatographic conditions, mass spectrometric parameters and sphingolipid MRM methods were defined previously (Tellier *et al.*, 2014). MRM methods used for phospholipids (PCs, PEs, PIs, PGs, PSs and phosphatidic acids (PA)) and galactolipids (MGDGs and DGDGs) were reported in supplementary material (Supporting Information Table S1).

Results

Global profiling and clustering of all the proteins identified and quantified in Arabidopsis autophagy mutants and control plants

The shotgun LC-MS/MS proteome analyses performed on autophagy defective lines (*atg5* and *atg5/sid2*) and their cognate control lines (Col and *sid2*), permitted to identify 2334 proteins that were quantified by XICs, and 89 proteins quantified with a spectral counting (considering SC > 4). The 2334 XICs quantified proteins identified were clustered in six different groups as shown in Fig. 1. Clusters 1 and 2 present proteins with lower concentrations in *atg5* mutants (*atg5* and *atg5/sid2*) relative to their respective controls (Col and *sid2*). Clusters 3 and 4 include proteins accumulated in *atg5* and *atg5/sid2* relative to Col and *sid2*. In cluster 3, protein accumulation was exacerbated under low nitrate (low-N) and under low sulfur (low-S) conditions. In cluster 4, the effect of the *sid2* genetic background on protein abundance was observed in all the growth conditions. In cluster 2, it was only observed under low-S conditions. In clusters 5 and 6 protein abundances in *atg5* and *atg5/sid2* were not different to that of their control lines.

The main predicted location of proteins of clusters 1 and 2 is chloroplast. The KEGG and gene ontology (GO) terms of cluster 1, related to amino acid (serine, glycine, arginine, lysine, valine, isoleucine), fatty acid, starch and glucose biosynthesis are significantly enriched in wild-type (Table S2). The KEGG and GO terms of cluster 2, related to photosystems I and II, porphyrin biosynthesis, glycolysis and neoglucogenesis, fatty acid biosynthesis, pentose phosphate and tricarboxylic acid cycle (TCA) pathways, amino acid (serine, glycine, arginine, lysine, valine, isoleucine) biosynthesis, and ribosome biogenesis are also significantly enriched in wild-type (Table S3). The KEGG and GO terms of the cluster 3, related to C metabolism (TCA, pentose phosphate, glycolysis), N metabolism (ammonium assimilation, amino acid degradation), S metabolism (glutathione, methionine biosynthesis, sulfur transfer), α-linoleic acid metabolism, proteasome, endoplasmic reticulum (ER) response to misfolded proteins, and peroxisome metabolism are significantly enriched in *atg5* and *atg5/sid2* (Table S4). Proteins of cluster 3 are mainly predicted in the mitochondria, peroxisome and vacuole. The KEGG and GO terms of the cluster 4, related to amino acid and fatty acid metabolisms, and to protein processing in the ER are significantly enriched in *atg5* and *atg5/sid2* (Table S5). GO terms of cluster 4 are also related to plant immunity, systemic acquired resistance and hypersensitive response. This explains the *sid2*-related effect observed in cluster 4. Proteins of cluster 4 are mainly predicted in the endomembranes and ER.

GO terms of cluster 5 and 6 are not described here as they do not show any difference related to the *atg5* mutation.

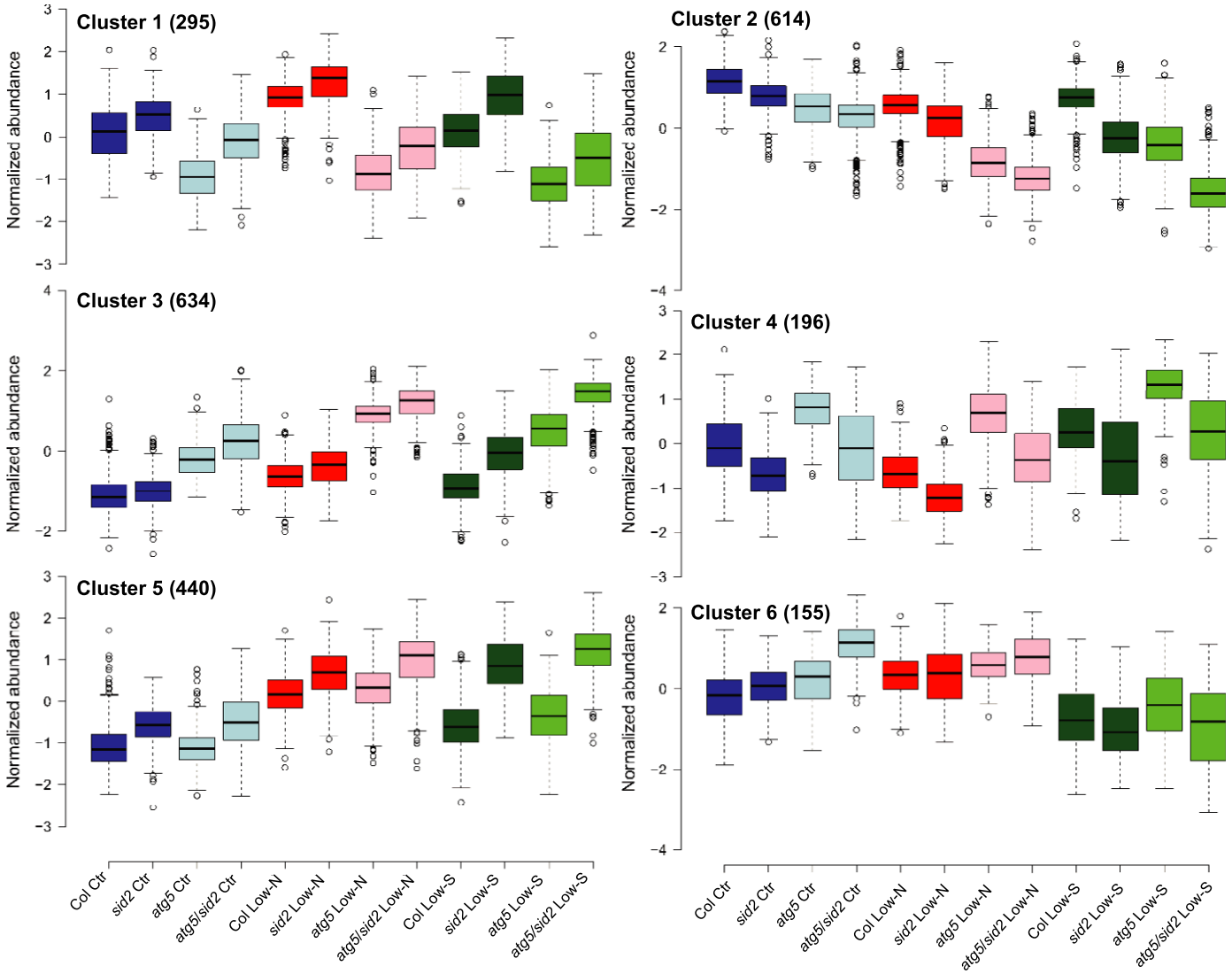

Fig. 1 Clustering of the 2334 XICs quantified proteins according to their abundances in each Arabidopsis genotype. Proteins were clustered according to their abundances in the Col, *sid2*, *atg5* and *atg5/sid2* genotypes, under control (Ctr, blue), low nitrate (Low-N, red) and low sulfur (Low-S, green) growth conditions. Dark blue, red or green colours represent controls (Col and sid2) and light blue, red or green colours represent *atg5* mutants in the Col and *sid2* backgrounds. The XICs abundance values were normalised to the median in GENESIS software (v.1.8.1; Sturn *et al*., 2002), and visualised as BoxPlots in BoxPlotR (Spitzer *et al*., 2014). BoxPlots present ± 1.5 median (middle), first (top) and last (bottom) quartiles; bars indicate interquartile range.

Identification of SA-independent and differentially expressed proteins in *atg5* mutants

ANOVA and Tukey tests were performed to identify the protein abundances significantly modified in *atg5* vs Col and in *atg5/sid2* vs *sid2* (Table S6).

Venn diagrams show that the number of the proteins significantly more or less abundant in *atg5* or *atg5/sid2* is much higher under low-N and low-S than under control (Ctr) growth conditions (Fig. 2a–c). The intersections between *atg5* vs Col and *atg5/sid2* vs *sid2* include proteins with abundance significantly modified in *atg5* in a SA-independent manner.

As our aim was to identify autophagy effects irrespective of SA effects, only the 1236 proteins present in the intersections of the Venn diagrams in Fig. 2(a–c) were considered for further analyses (Fig. 2d; Table S7). Note that 1237 proteins are represented in Fig. 2(d), as one protein (corresponding to AT2G03440) was counted twice due to its opposite change under Ctr and low-N conditions. A large part of the 1236 proteins identified was common to at least two growth conditions. The proteins with lower abundance in both *atg5* and *atg5/sid2* under Ctr, low-N or low-S conditions were predicted in the chloroplast and in the extracellular space (Fig. 3) The more abundant proteins were predicted in the cytosol, ER, Golgi, mitochondria and peroxisome (Fig. 3). Although the number of these proteins increased under starvations (both low-N and low-S), their repartition in the different subcellular locations were mainly conserved under each growth condition as shown in Fig. S1. It should be noted that for 1182 proteins among the 1236 identified in Table S7, transcript levels were not different between *atg5* mutants and control lines,

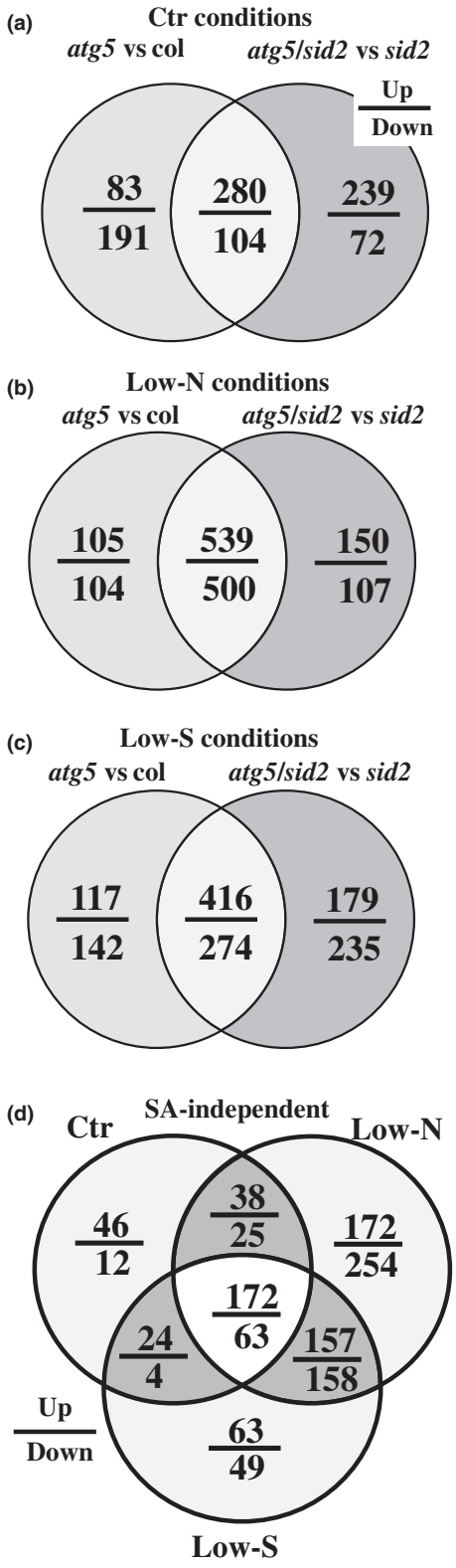

Fig. 2 Venn diagrams highlight the salicylic acid (SA)-independent changes in the *atg5* Arabidopsis mutant under the three growth conditions. Proteins significantly modified in *atg5* mutants are shown for control (a; Ctr), Low-N (b) and Low-S (c) conditions. Light grey intersections in (a), (b) and (c) contain proteins modified in *atg5* in a SA-independent manner. The Venn diagram represented in (d) considers only the 1236 proteins significantly differentially regulated in a SA-independent manner in (a), (b) and (c) under Ctr, low-N and low-S conditions. The upper and the lower numbers indicate the numbers of significant up- and downregulated proteins, respectively. Significant protein and statistics are presented in Supporting Information Table S6.

regardless of the growth conditions. The 54 proteins that were modified at both transcript and protein levels were mainly related to senescence and biotic or abiotic stresses. Their transcript levels and protein abundances were generally higher than in control lines, especially under low-N conditions (Table S7).

Bioinformatics study of the potential function of the proteins differentially accumulated in *atg5* in a SA-independent manner

Bioinformatics analyses first focused on the core list (CL) containing the 235 proteins differentially accumulated in *atg5* in a SA-independent manner irrespective to growth conditions (Fig. 2d). Furthermore, the full list (FL) of the proteins differentially accumulated in a SA-independent manner (Fig. 2d; Table S7), in at least one of the three conditions, was analysed, to determine the similarities and the specificities related to each growth condition.

The CL, which includes 172 upregulated and 63 downregulated proteins, represents the protein abundance hallmark of autophagy defects (Table S8). Significant functional categories of CL are related to sugar and carbohydrate metabolisms (photosynthesis, glycolysis, TCA pathway, major and minor carbohydrate (CHO) pathways), to redox pathway, to lipid and amino acid metabolisms and catabolisms, to protein degradation, to the fatty acid degradation and β-oxidation pathway (Fig. S2; Table S8). Interestingly, the same functional categories were significantly identified from FL (Fig. 4). The proportions of up- and down-proteins in each functional category were mostly similar in the CL and the FL.

Although CL proteins represented 19% of the FL proteins, the CL proteins with predicted location in ER, peroxisome and Golgi represented 49%, 49% and 29% of the FL proteins, respectively (Fig. 4c). This means that a large proportion of the ER, peroxisome and Golgi proteins in the FL were significantly differentially accumulated in *atg5* and *atg5/sid2* independently of the growth conditions. In addition, almost all the ER-, Golgi- and peroxisome-predicted proteins identified in CF and FL were more abundant when *atg5* was mutated. By contrast the vacuole-, extracellular-, chloroplast- and mitochondrion-predicted proteins were highly under-represented in the CL relative to the FL. This indicated that these proteins were differentially accumulated in *atg5* and *atg5/sid2* relative to controls depending on low-N or low-S growth conditions (Table S7). The low-N specific proteins were much more numerous than those specific of Ctr or low-S conditions (Fig. 2d). The only GO term significantly enriched in the low-N specific protein of *atg5* and *atg5/sid2* was related to glycoside hydrolases (Table S9). We could, however, notice the large number of proteases overaccumulated in *atg5* and *atg5/sid2* under low-N specifically, that reflected the changes reported by Havé *et al.* (2018) and the inability of autophagy mutants to

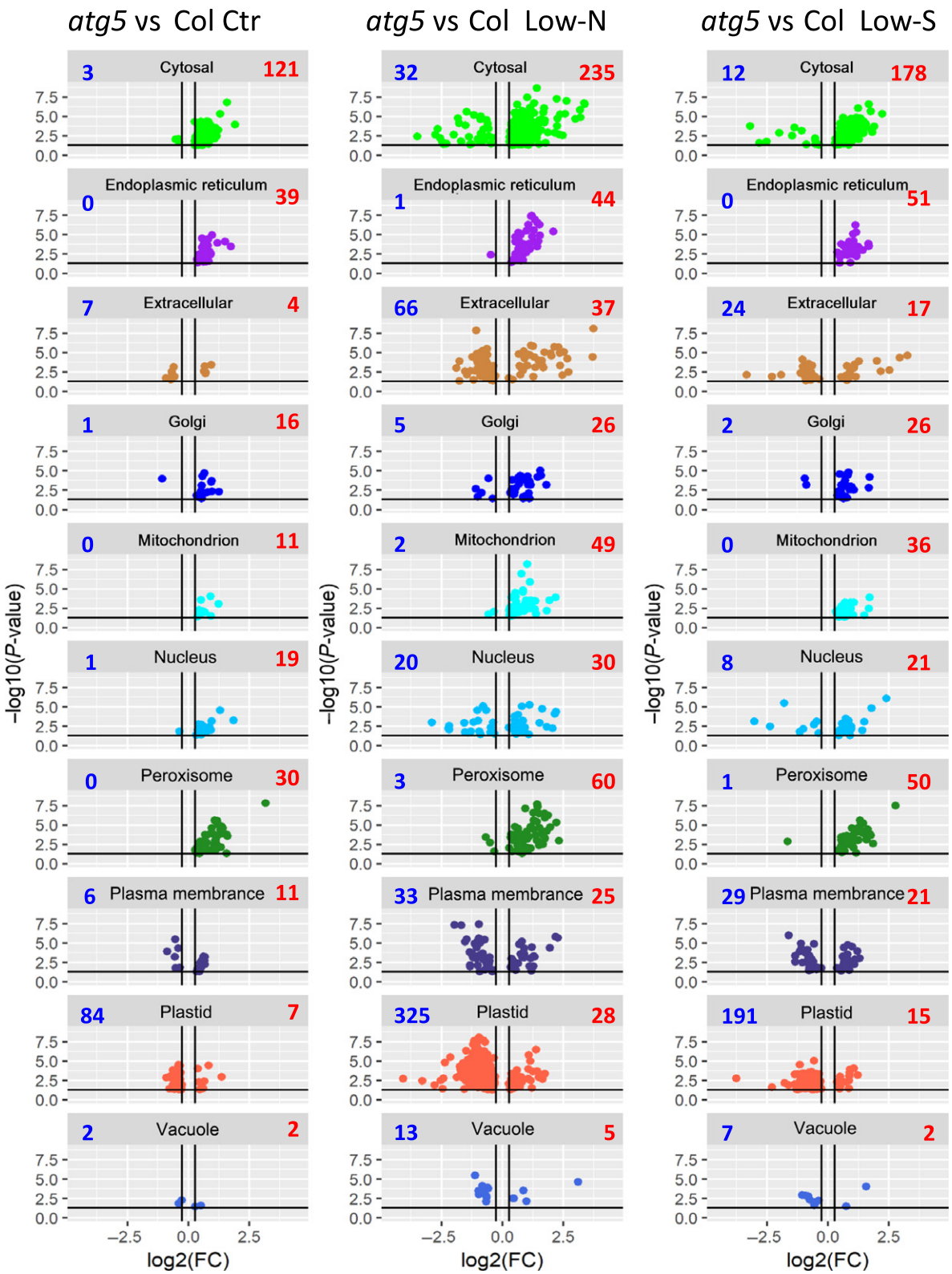

Fig. 3 Volcano plot of the predicted localisation of the 1236 proteins significantly modified in both *atg5* and *atg5/sid2* Arabidopsis mutants. Volcano plots of proteins modified under control (Ctr), Low-N and Low-S growth conditions are shown. *X*-axis represents the $\log_2$ of the fold change (FC) of the *atg5* vs Col comparison. *Y*-axis represents the significance of the changes calculated from the *P*-value. The red and blue numbers in the subfigures represent the numbers of proteins significantly more or less abundant in *atg5* in a salicylic acid (SA)-independent manner. Significant proteins are shown in Supporting Information Table S6.

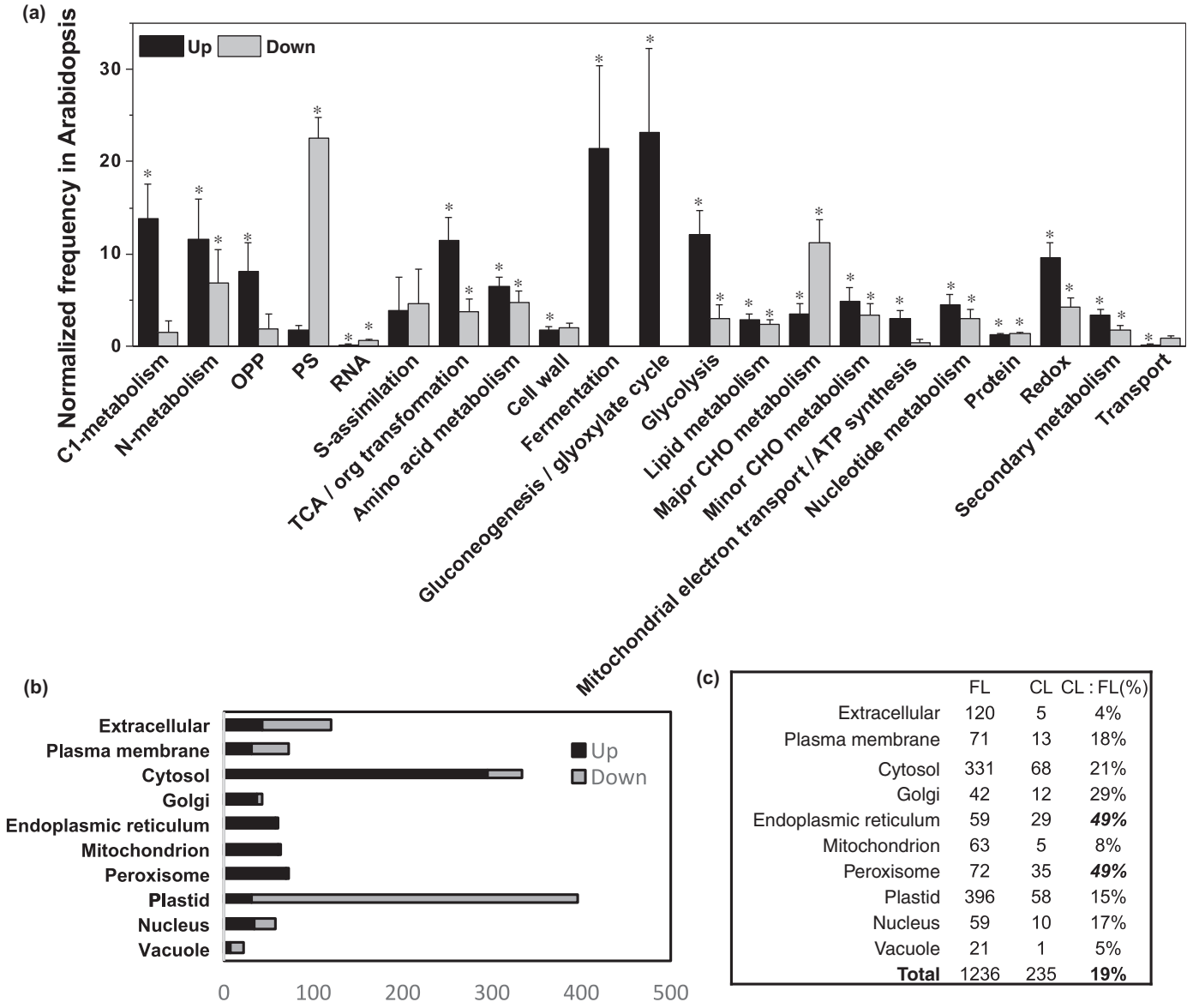

	FL	CL	CL : FL(%)
Extracellular	120	5	4%
Plasma membrane	71	13	18%
Cytosol	331	68	21%
Golgi	42	12	29%
Endoplasmic reticulum	59	29	***49%***
Mitochondrion	63	5	8%
Peroxisome	72	35	***49%***
Plastid	396	58	15%
Nucleus	59	10	17%
Vacuole	21	1	5%
Total	1236	235	**19%**

Fig. 4 Functional categories and predicted localisations of the full list (FL) of Arabidopsis proteins. The FL contains all the proteins significantly more of less abundant in *atg5* in a SA-independent manner under control, low-N or low-S conditions. (a) Frequency of the functional categories of the FL proteins are presented. *Y*-axis represents the frequency of each functional category normalised to the Arabidopsis genome. Bars, SD for 100 bootstraps. Functional categories were determined using Classification SuperViewer tool in BAR database (http://bar.utoronto.ca/welcome.htm). * Indicate that the *P*-value of hypergeometric distribution is < 0.05. (b) The number of proteins more abundant in both *atg5* and *atg5/sid2* are presented in red, and the less abundant proteins in blue. The predicted subcellular locations were analysed using SUBA4. (c) The number of proteins from the full list (FL) and from the core list (CL) predicted in each cell compartment and their ratio as CL : FL (in %) are presented. Bold and italic % indicate the highest CL : FL ratios.

manage N resources properly especially when nitrogen is scarce (Guiboileau *et al.*, 2013). The GO terms of the few low-S specific proteins were mainly characterised by significant enrichment in aquaporins.

Autophagy mutant displays typical hallmarks of ER stress and peroxisome catabolic pathway

Among the 59 ER proteins differentially expressed in *atg5* and *atg5/sid2* vs Col and *sid2*, many protein disulfide-isomerase (PDIL) thioredoxins were more abundant in *atg5* lines suggesting strong ER stress (Fig. 5; Table S7). The accumulation of luminal HSP70 and HSP90 chaperones, enzymes involved in protein glycosylation/glucosylation and protein folding, and ERAD (endoplasmic reticulum associated protein degradation) related proteins in *atg5* and *atg5/sid2* confirmed ER stress (Table S7). As these hallmarks were found irrespective of growth conditions, we deduce that ER stress is the most remarkable cell disorder engendered by autophagy dysfunction (Fig. 5). The higher abundance of several ER membrane-proteins as OST/ribophorin and reticulon in autophagy mutants emphasise the role of autophagy in ER maintenance. Interestingly, several ER-to-Golgi vesicle-mediated

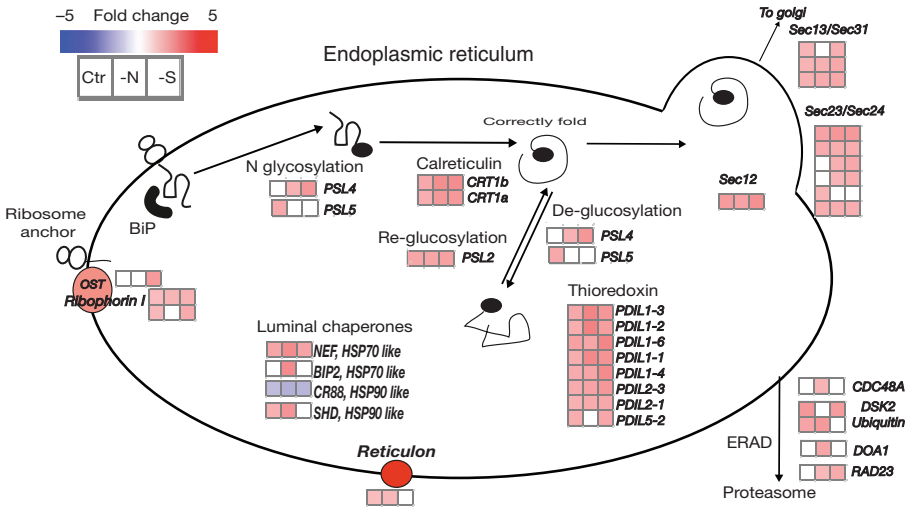

Fig. 5 Protein changes in the endoplasmic reticulum of autophagy Arabidopsis mutants. For each significant protein, fold changes (FC) are presented as heat maps with shades of red or blue colours according to the scale bar. The heat map squares represent the FC values of the control (Ctr), the low-N and the low-S conditions. Data are the mean of the FC of *atg5* vs Col and *atg5/sid2* vs *sid2*. Data are presented in Supporting Information Table S7.

transport proteins, belonging to the Sec12, Sec23/Sec24 and Sec13/Sec31 complexes, were more abundant in the *atg5* lines, showing that the ER-to-Golgi vesicular pathway was more solicited in autophagy mutants than in control lines.

In peroxisome, superoxide dismutases (CSD1 and CSD3), *S*-nitrosoglutathione reductase (GSNOR) and catalases (CAT1, 2 and 3), that regulate oxidative stress were more abundant in *atg5* and *atg5/sid2* (Fig. 6; Table S7). Surprisingly, the increase of the relative abundance of the three catalases was higher under the control conditions than under low-N, and undetectable under low-S. Results then showed that by comparison with control lines, the oxidative stress affecting *atg5* mutants was more severe under control conditions than under low-N and low-S.

The peroxisome enzymes involved in the degradation of branched chain amino acids (BCAA) and of glycine, serine and threonine and the YLS4 aspartate amino transferase 3 involved in the degradation of asparagine and aspartate, were more abundant in *atg5* and *atg5/sid2* (Table S10). Although enzymes involved in AA catabolism in the cytosol and mitochondria (Hildebrandt *et al.*, 2015) were also more abundant in *atg5* and *atg5/sid2*, they were more specifically increased under low-N or low-S, while peroxisome catabolic enzymes were found irrespective of the growth conditions (Table S10). This may be explained by the fact that the BCAA degradation pathway is connected to fatty acid β-oxidation through the involvement of the acyl co-enzyme A oxidases (ACX) and the 3-ketoacyl-CoA thiolase (KAT) in the peroxisome (Hildebrandt *et al.*, 2015; Fig. 6). Accordingly, peroxisome enzymes participating in fatty acid (FA) β- and α-oxidation were more abundant in *atg5* and *atg5/sid2* (Fig. 6). The overaccumulation of malate dehydrogenase and citrate synthase attested that glyoxylic cycle was stimulated in *atg5* mutants.

Chloroplastic proteins are less abundant in *atg5* and *atg5/sid2* under nutrient limitations

Almost all the 396 chloroplast-predicted proteins were less abundant in *atg5* and *atg5/sid2* than in control lines under low-N and low-S conditions (Table S7; Fig. 7). Most of these were not modified under control conditions. These proteins are involved in photosynthesis, Calvin cycle and FA biosynthesis (Fig. 7). Their lower abundance may explain why *atg* mutants were found depleted in sugar and starch in previous studies (Guiboileau *et al.*, 2013; Masclaux-Daubresse *et al.*, 2014). The lower abundance of chloroplast ribosomal proteins (RP) and chloroplast tRNA ligases in *atg5* and *atg5/sid2* attests of a global decrease of protein translation in their chloroplasts (Fig. S3; Table S7). Like the photosynthetic apparatus, ribosomes constitute a large nitrogen reservoir in leaf tissues, which can be remobilised under N starvation. Decrease in chloroplast proteins is then in good agreement with the increase of amino acid catabolism reported above.

Although most of the chloroplast proteins were less abundant in *atg5*, it is noteworthy that three chloroplast-predicted proteins significantly accumulated in *atg5* and *atg5/sid2* irrespective of the growth conditions. They are the β-amylase 1 (BAM1) involved in starch degradation, the FBA5 (FRUCTOSE-BISPHOSPHATE ALDOLASE 5) isoenzyme probably involved in Calvin cycle and the TPP2 serine protease involved in protein degradation.

Changes in cytosolic, mitochondria and extracellular proteins in *atg5* and *atg5/sid2* are more important under low-N conditions

The cytosolic proteins differentially accumulated in *atg5* and *atg5/sid2* were predominantly found under low-N conditions, and in a lower extent under low-S (Table S7; Fig. 4). Most of them were more abundant in *atg5* mutants and involved in carbon primary and secondary metabolisms, in protein degradation (see Havé *et al.*, 2018 for details), and in pentose phosphate and glycolysis pathways. Among the few cytosolic proteins less abundant in *atg5* and *atg5/sid2*, the cytosolic RP displayed strong decrease relative to control lines under low-N conditions. Most of the mitochondria-predicted proteins identified were more abundant in *atg5* and *atg5/sid2*, and mostly found under nutrient limiting and especially low-N conditions (Table S7; Fig. S4). They are involved in citrate cycle (TCA)

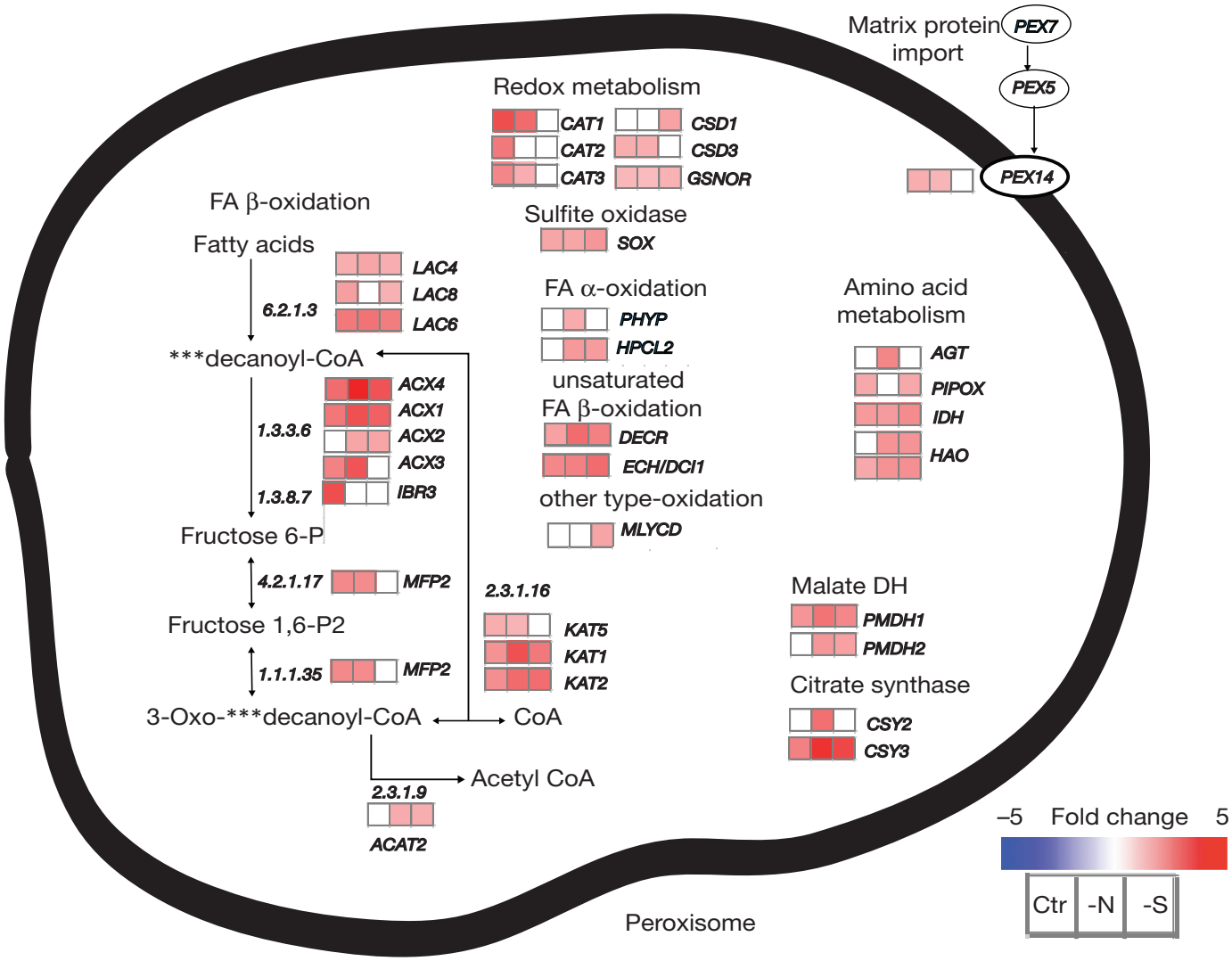

Fig. 6 Protein changes in the peroxisome of autophagy Arabidopsis mutants. For each significant protein, fold changes (FC) are presented as heat maps with shades of red or blue colours according to the scale bar. The heat map squares represent the FC values of the control (Ctr), the low-N and the low-S conditions. Data are the mean of the FC of *atg5* vs Col and *atg5/sid2* vs *sid2*. Data are presented in Supporting Information Table S7.

and in mitochondria electron transport. Therefore, the abundance of cytosolic and mitochondria proteins suggests that pentose phosphate pathway, glycolysis and TCA are more active in *atg5* lines under nutrient limiting conditions (Fig. S4), which is in good agreement with the decrease of photosynthesis and the changes observed for chloroplast proteins.

The extracellular-predicted proteins represent the third largest list of proteins differentially accumulated in a SA-independent manner in *atg5* mutants relative to control plants (Table S7). However only 4% of them are found in all the three growth conditions (Table S8). Changes in extracellular-predicted proteins are mostly found under low-N conditions. The extracellular proteins identified were generally involved in cell wall modifications (mostly less abundant in *atg5*), protein degradation (less abundant in *atg5*, see Havé *et al.*, 2018) and response to biotic stress like the PR1, PR4 and PR5 pathogenesis-related proteins (more abundant in *atg5*).

Acyl-lipid metabolism is significantly modified in autophagy mutants

Large modifications of amino acid, sugar and starch metabolisms in the rosettes of autophagy mutants have been previously reported (Guiboileau *et al.*, 2013; Izumi *et al.*, 2013b; Masclaux-Daubresse *et al.*, 2014). Our proteome study confirms the strong effect of the *atg5* mutation on the amino acid (Fig. S5; Tables S7–S10) and lipid catabolism as changes found in the ER and peroxisome proteins were found irrespective of nutritive conditions (Figs 5, 6). Therefore, modifications impacting acyl-lipid metabolism were investigated.

Total FA, originating from membrane and storage lipids, were determined using GC-MS after total lipid extraction (Fig. S6). Marked genotype-dependent differences were revealed, especially for long chain fatty acids (LCFA) and very long chain fatty acids (VLCFA) (Fig. S6). This prompted us to undertake LC-MS-based lipidomic approaches targeting more specifically

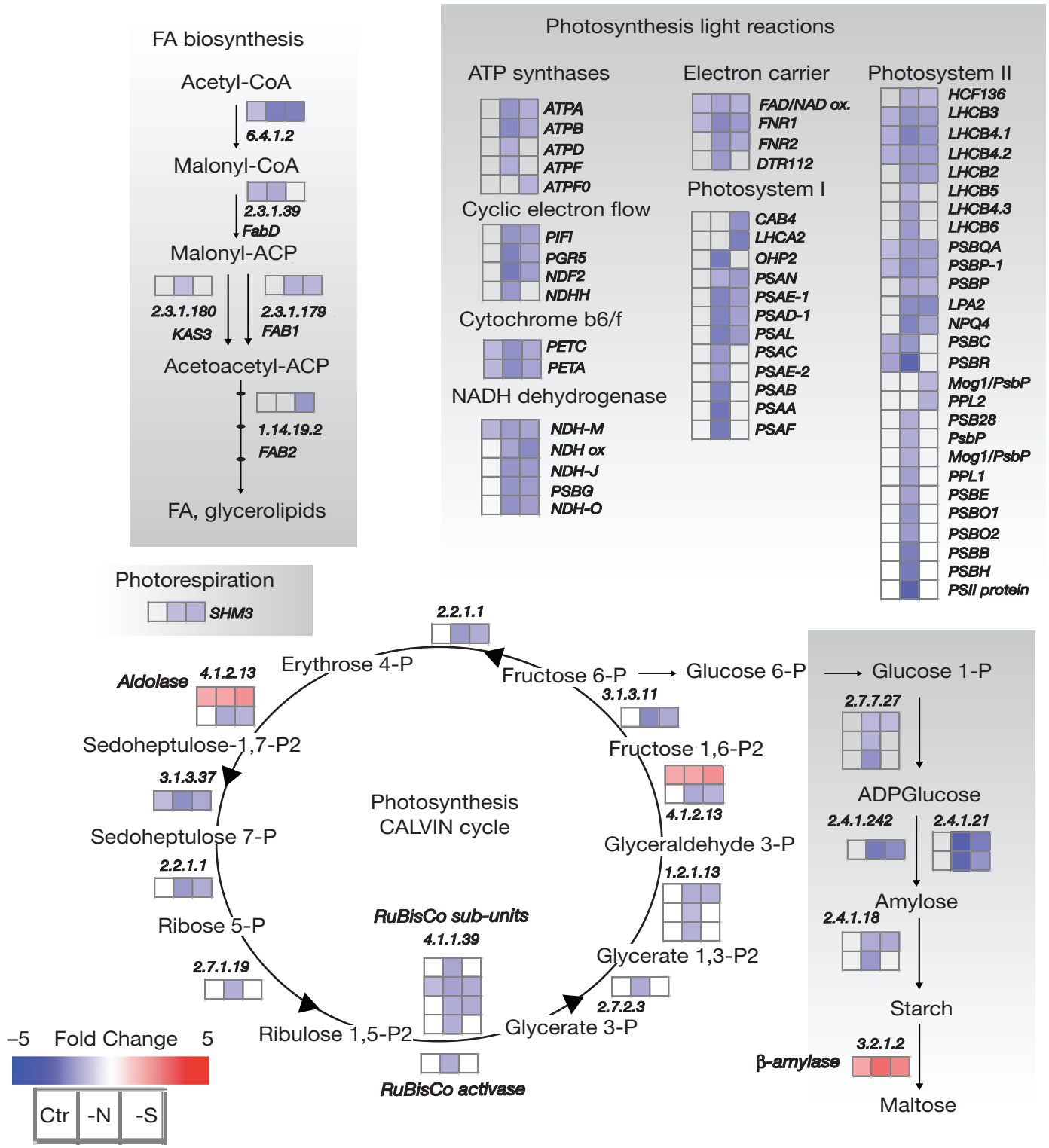

Fig. 7 Protein changes in the chloroplasts of autophagy Arabidopsis mutants. For each significant protein, fold changes (FC) are presented as heat maps with shades of red or blue colours according to the scale bar. The heat map squares represent the FC values of the control (Ctr), the low-N and the low-S conditions. Data are the mean of the FC of *atg5* vs Col and *atg5/sid2* vs *sid2*. Data are presented in Supporting Information Table S7.

phospholipids, galactolipids, sphingolipids and triacylglycerols (Figs 8, S7, S8; Table S11).

Phospholipids form a large family of glycerolipids, mainly composed of phosphatidylcholine (PC), phosphatidylethanolamine (PE), phosphatidylglycerol (PG), phosphatidylinositol (PI), phosphatidylserine (PS) and PA. Overall, phospholipid compositions and levels were strongly altered in autophagy defective lines (Figs 8, S7; Table S11). All the major molecular species of PC, the

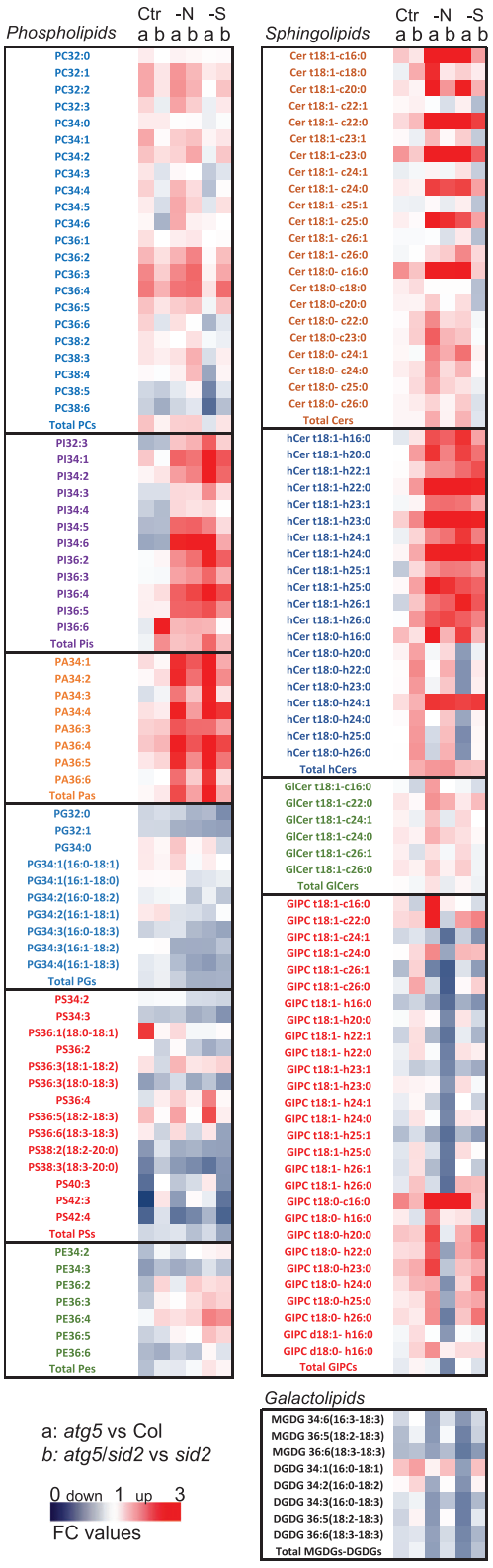

Fig. 8 Lipid changes in autophagy Arabidopsis mutants. Fold changes between *atg5* vs Col (a) and *atg5/sid2* vs *sid2* (b) are shown under control, low-N (−N) and low-S (−S) conditions as heat maps with shades of red or blue colours according to the scale bar. Phosphatidylcholine (PC), phosphatidylinositol (PI), phosphatidic acid (PA), phosphatidylglycerol (PG), phosphatidylserine (PS) and phosphatidylethanolamine (PE) represent phospholipids. Ceramides (Cers), hydroxyceramides (hCers), glucosylceramides (GlCers) and glycosyl-inositol-phosphoryl-ceramides (GIPC) represent sphingolipids. MGDG and DGDG are galactolipids. Fold changes were obtained from data (means of concentrations and SD) presented in Supporting Information Table S11.

most abundant membrane phospholipid, accumulated in *atg5* and *atg5/sid2* lines under control, low-N and low-S conditions, although in a lower extent under low-S. The minor phospholipids, PI and PA, showed a similar behaviour, with higher concentrations in *atg5* and *atg5/sid2* when compared with their controls under low-N and low-S conditions (Fig. S7B,C). By contrast, PS and PG levels decreased significantly in *atg5* and *atg5/sid2* under all the growth conditions (Fig. S7D,E). Finally, there was almost no change in the concentration of PEs except the significant decrease in PE34:3 and increase of PE36:4 and PE36:5 in *atg5* and *atg5/sid2*, essentially under the control conditions (Fig. S7F).

The profiling of galactolipids provided consistent data with the proteomic analyses that indicated a decrease in chloroplast protein steady-state levels. Indeed, the two main classes of galactolipids, mono- and di-galactoyldiglycerides (MGDG and DGDG), were lower in *atg5* and *atg5/sid2* with regard to their respective controls, with the exception of the molecular species 34 : 1 (16 : 0 18 : 1) of DGDG that increased (Fig. 8; Table S11). Changes observed in galactolipid compositions could explain the observed changes in the specific FAs C16:0, C16:3 and C18:3 under the same conditions (Fig. S6). Both chloroplast protein and galactolipid decreases could reflect higher degradation of chloroplasts or lower chloroplast number in *atg5* mutants.

Sphingolipids are composed of four classes: ceramides (Cers), hydroxyceramides (hCers), glucosylceramides (GluCers) and glycosyl-inositol-phosphoryl-ceramides (GIPC), (Fig. S8). Although generally not significantly modified under control conditions, the Cers and hCers strongly increased in *atg5* and *atg5/sid2* relative to controls under low-N and low-S conditions (Figs 8, S8). By contrast, GluCer levels were unaffected irrespectively of the genotype and growth conditions. Likewise, levels of the two main molecular species of GIPC (t18:1-h24:0 and t18:1-h24:1) were not affected by autophagy (Table S11), while their hydroxylated and nonhydroxylated precursors were sharply accumulated under similar conditions (Fig. S8). One specific molecular species of GIPC, t18:0-C16:0, strongly increased in *atg5* and *atg5/sid2* whereas others like t18:1-h16:0 showed an opposite behaviour (Fig. S8).

The purification of triacylglycerol (TAG) using thin layer chromatography was assayed. We could not find any substantial amount of TAG in any of the four genotypes and whatever growth conditions, to perform deeper GC-MS analyses. This means that TAGs were scarce and did not accumulate in any plants.

Discussion

The transcriptome of *atg5* and WT plants performed few years ago by Masclaux-Daubresse *et al.* (2014) and in the present study under low-S, showed that the most striking change observed at

transcript levels was the over-expression in *atg5* of biotic and abiotic marker genes and of genes involved in the SA and JA signaling pathways. The transcriptome of *atg5* reflected modifications in the anthocyanin, methionine and glutathione metabolic pathways, that were confirmed by metabolomic analyses (Masclaux-Daubresse *et al.*, 2014). Recently McLoughlin *et al.* (2018) confirmed flavonoids modifications in the *atg12* maize mutant that were also associated to changes in the abundance of the transcript of their biosynthetic enzymes.

Interestingly, our proteomic analysis shows that the changes in protein abundance in *atg5* and *atg5/sid2* were generally not related to significant changes in their mRNA steady-state level. Among the 1236 proteins modified in *atg5* in a SA-independent manner, only 54 were identified in *atg5* transcriptome analyses, mainly under low-N. These 54 proteins are mostly related to leaf senescence and biotic/abiotic stresses. Changes in *atg5* proteome then appear mostly related to protein stability and to primary metabolism. Changes in *atg5* transcriptome seem more related to stress responses and to secondary metabolites that play a role in plant defence or tolerance to stresses.

Changes in proteins and lipids suggest smaller or less abundant chloroplasts in autophagy mutants

Chloroplast proteins and galactolipids were less abundant in *atg5* and *atg5/sid2* than in controls under nutrient limiting conditions (low-N and low-S). This suggested that chloroplasts were smaller or less abundant in *atg5* mutants than in control lines. The fact that the decrease of chloroplast proteins was exacerbated under low-N especially, was in good agreement with the higher protease abundances and activities reported by Havé *et al.* (2018) in *atg5*, that reflected the emergence of alternative autophagy-independent pathways for N-recycling and possibly chloroplast degradation. The increase in the amount of the PATATIN-LIKE PROTEIN 2 (PLP2) and α-DIOXYGENASE-1 (α-DOX1), that can degrade a wide range of substrates including phospholipids and galactolipids, is in line with this assumption (La Camera *et al.*, 2005, 2009; Fig. 9). Interestingly, lower chloroplast protein and lipid levels were also reported in the *atg12* maize mutant by McLoughlin *et al.* (2018). Chloroplasts are the major nitrogen reservoirs in leaves. The amount of chloroplast protein is strongly associated and adapted to nitrogen availability. The fact that nitrogen recycling from chloroplast is more intense in *atg5* may explain why autophagy mutants are hypersensitive to nitrogen limitation and display earlier senescence. In line with this, the lower ribosomal protein abundance *atg5* under N limiting conditions is not surprising as ribosome constitute another substantial nitrogen reservoir in the cell.

ER stress and peroxisome β-oxidation are related to dramatic lipid modifications

Irrespective of the nutritive conditions and of the SA effects, the strongest change in *atg5* was the accumulation of ER- and peroxisome-localised proteins.

ER stress markers, like BiP, CNX, CRT and PDIL, were largely over-accumulated in *atg5* and *atg5/sid2* (Fig. 5; Howell, 2013; Cacas, 2015). This corroborated the activation of ER stress found in mammal, yeast and plant autophagy mutants, and the fact that autophagy alleviates ER stress by eliminating misfolded proteins (Bernales *et al.*, 2006; Ogata *et al.*, 2006; Yorimitsu *et al.*, 2006; Ding *et al.*, 2007; Kouroku *et al.*, 2007; Munch *et al.*, 2014; Rashid *et al.*, 2015; Cai *et al.*, 2016; Yang *et al.*, 2016; Bao *et al.*, 2018). Liu *et al.* (2012) showed in Arabidopsis that autophagosomes can contain ER membranes, which suggested a role in lipophagy. ER membranes are mainly constituted of phospholipids. They are also a source of lipids for building the pre-autophagosomal structures and for autophagosome expansion (Le Bars *et al.*, 2014). Autophagy is then crucial in ER membrane recycling and more generally in ER quality control.

The fact that proteomic analysis reveals an accumulation of peroxisome proteins in *atg5* and *atg5/sid2* could reflect a lower pexophagy rate in autophagy mutants, as suggested by McLoughlin *et al.* (2018). However, the fact that many of the overaccumulated peroxisomal proteins are dedicated to the amino acid and lipid catabolisms is in good accordance with the decay of chloroplast and a role of β-oxidation in alternative energy supply. The increase of β-oxidation is also in good agreement with the increase of TCA and gluconeogenesis proteins in mitochondria and cytosol, respectively. It is then liable that a sizable portion of peroxisomes in the leaves of *atg5* mutants works as glyoxysomes that provide energy and carbon skeletons in a cellular context where photosynthesis in chloroplasts is weak (Shibata *et al.*, 2013; Zientara-Rytter & Subramani, 2016). The fact that both ATP and ADP levels were maintained in *atg5* (data not shown) supports this hypothesis.

Both the ER and peroxisome are known to play a crucial role in lipid homeostasis (Fig. 9). While peroxisomes are involved in FA degradation through β-oxidation cycle as aforementioned, the ER is the subcellular site where phospholipid, sterol and TAG are synthesised. ER is involved in VLCFA elongation and initiates sphingolipid production. In leaves, lipid droplet (LD) biogenesis occurs at the ER membrane via a budding mechanism that releases into the cytoplasm vesicles delineated by a proteo-phospholipid-composed hemi-membrane that contain TAGs. Interestingly, we found that the PDAT1 protein (PHOSPHOLIPID-DAIACYLGLYCEROL ACYL-TRANSFERASE-1) was significantly increased in *atg5* irrespective of the growth conditions (Fig. 9). PDAT1 is known to be responsible for TAG production via a membrane remodelling mechanism in stressed photosynthetic material (Boyle *et al.*, 2012; Tjellstrom *et al.*, 2015; Mueller *et al.*, 2017). Its increase supports the hypothesis of a higher TAG and LD production from the ER in *atg5*. However, the thin layer chromatography we performed to purify and quantify TAGs showed that these molecules were undetectable regardless of genotypes and growth conditions. Reasoning that β-oxidation was activated in *atg5* and *atg5/sid2*, we supposed that the faint steady-state levels of TAG, that is below the limit of detection, was due to the high glyoxysome catabolic activity (Figs 9, 10). If accumulation of TAG

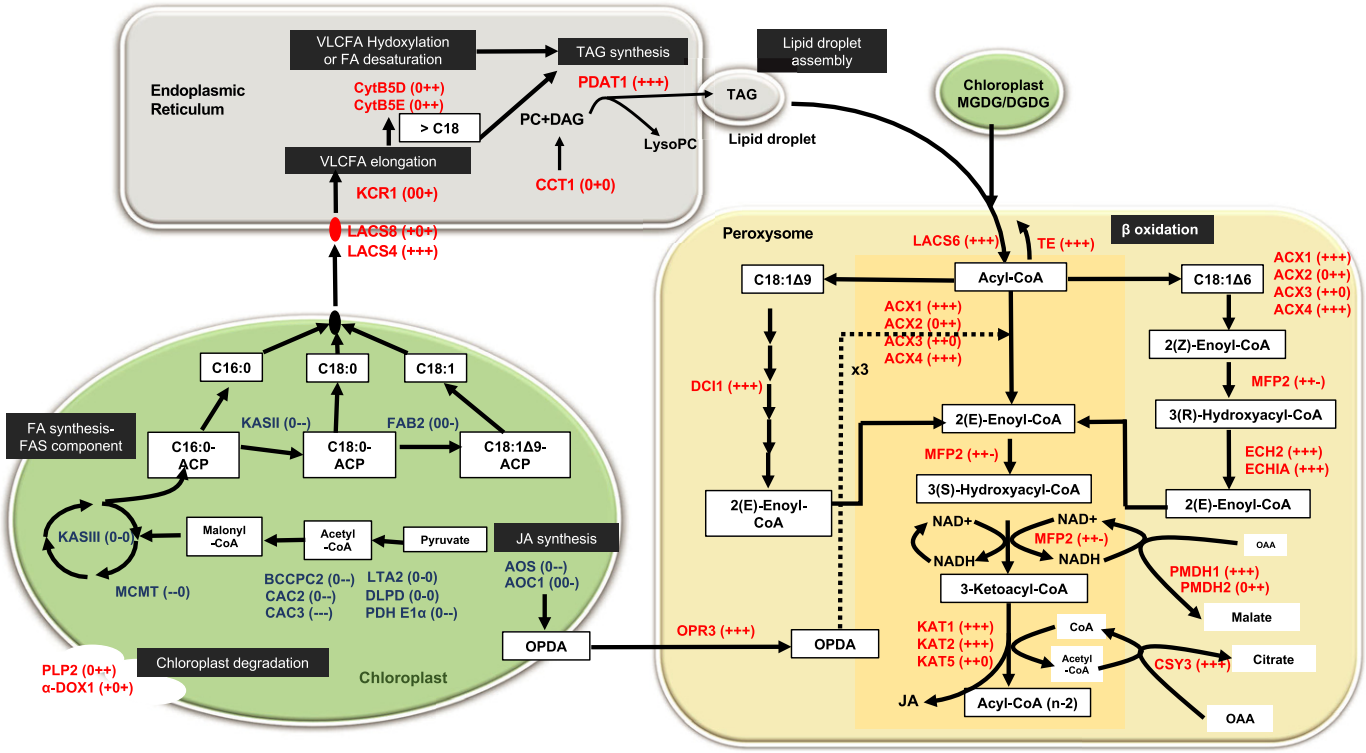

Fig. 9 Lipid recycling in autophagy-deficient Arabidopsis mutant. Under restful or stressful conditions, long chain fatty acid neosynthesis, which is localised to plastids (defining the 'prokaryotic pathway'), is either unaltered or downregulated in *atg5* mutants at the protein levels. By contrast, the steady-state levels of the endoplasmic reticulum (ER)-localised long chain acyl-CoA synthetase 4 (LACS4) is constitutively up-regulated in any conditions, indicating that potentially more long chain acyl-CoA are elongated in the ER in mutants. This is coherent with our fatty acid (FA) dosage showing a significant increase in specific very long chain fatty acids (Supporting Information Fig. S6). Remarkably, two cytochrome b5 isoforms (CytB5D & E) are also accumulating under both nitrogen- and sulfur-limiting conditions. Cytochrome b5 enzymes are known to be important reducing co-factors for very long chain fatty acid (VLCFA) hydroxylation or FA desaturation. Hydroxylated VLCFA obtained are likely to be incorporated to sphingolipids which were found to over-accumulate in *atg5* mutants (Fig. S8) whereas unsaturated FA are supposed to be esterified onto glycerol to form triacylglycerol (TAG). The increase in PHOSPHOLIPID-DIACYLGLYCEROL ACYLTRANSFERASE-1 (PDAT1) levels, irrespective of the physiological context, is all the more relevant to this last scenario and sustains the idea of lipid droplet (LD) production at the ER. In accordance with a possible TAG synthesis that would be delivered through LD to peroxisomes, most enzymes involved the β-oxidation cycle, in addition to the acyl-CoA synthetase LACS6, are upregulated in autophagy-deficient mutants in any considered conditions. Although β-oxidation could be dedicated to jasmonic acid synthesis, the latter requires only one the three pathways which are found activated in this study, arguing in favor of a lipid degradative process. The + or − signs following enzymes names indicates whether the protein level is upregulated or downregulated *atg5* lines when compared to wild-type plants under control, nitrogen and sulfur-limiting conditions, respectively. LCFA, long chain fatty acids; VLCFA, very long chain fatty acids; ACP, acyl-carrier protein; ACX 1-4, acyl-CoA oxidase 1-4; AOC, allene oxide cyclase; AOS, allene oxide synthase; BCCPC2, biotin carboxyl carrier protein 2; CAC2, acetyl co-enzyme A carboxylase biotin carboxylase subunit; CAC3, acetyl co-enzyme A carboxylase carboxyltransferase α-subunit; CCT1, phosphorylcholine cytidylyltransferase; CSY3, citrate synthase 3; DCI1, delta(3,5), delta(2,4)-dienoyl-CoA isomerase 1; DLPD, dihydrolipoyl dehydrogenases; ECH2, enoyl-CoA hydratase 2; ECHIA, enoyl-CoA hydratase/isomerase A; KASII, fatty acid biosynthesis 1; KASIII, 3-ketoacyl-acyl-carrier protein synthase III; KAT1, 4-5, keto-acyl co-enzyme A thiolase 1, 4-5; KCR1, β-ketoacyl reductase 1; FAB2, stearoyl-acyl-carrier-protein desaturase; LTA2, 2-oxoacid dehydrogenases acyltransferase; MCMT, malonyl CoA-acyl-carrier protein transacylase; MFP2, multifunctional protein 2; OPR3, oxophytodienoate-reductase 3; PDH E1, pyruvate dehydrogenase E1α; PMDH1-2, peroxisomal NAD-malate dehydrogenase 1-2; TE, thioesterase.

has been reported in *atg5*, it was only in Arabidopsis etiolated seedlings (Avin-Wittenberg *et al.*, 2015).

Endomembrane lipid recycling by autophagy

As said before, the marked decrease in the main chloroplast lipids, MGDG and DGDG, in *atg5* mutants (Fig. 8) suggests that plastid membranes can be used as a source for β-oxidation in autophagy mutants (Rottet *et al.*, 2015; Mueller *et al.*, 2017; Zechner *et al.*, 2017). Recycling of chloroplast membranes then appears independent of functional autophagy machinery.

Like Izumi *et al.* (2013a), we observed the accumulation of phospholipids in *atg5*. Phospholipids are mainly in extraplastidial membranes, and their accumulation clearly points autophagy as a key player in cell endomembrane homeostasis (Figs 8–10). Changes in sphingolipid compositions and the strong increase in Cers and hCers in *atg5* and *atg5/sid2* support this assumption. Although alteration of ceramide concentrations could be attributed to ER dysfunction, the changes observed in GIPC concentrations reflect modifications in plasma membrane properties. GIPC are indeed the main structural lipids of plasma membrane (Cacas *et al.*, 2016; Fig. 10).

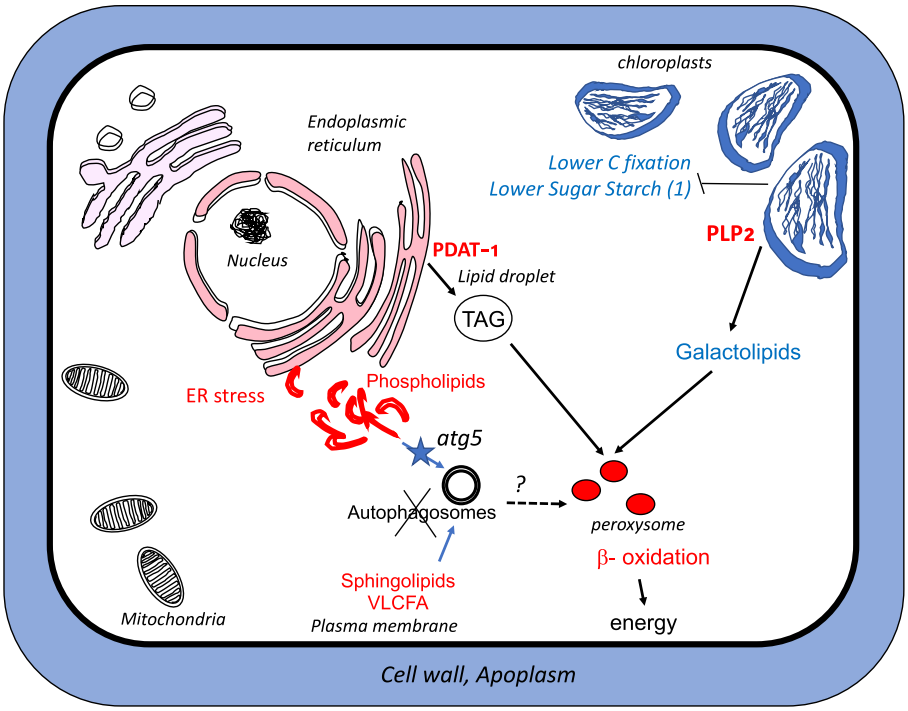

Fig. 10 Schematic representation of metabolic changes occurring in a leaf cell of the *atg5* Arabidopsis mutant. Red colour represents increases in protein contents and/or metabolic pathways in leaf tissues of *atg5*; Blue colour represents decreases in protein contents and metabolites in *atg5*. VLCFA, very long chain fatty acid; LD, lipid droplet; TAG, triacylglecerol; PDAT1, PHOSPHOLIPID-DIACYLGLYCEROL ACYLTRANSFERASE-1; PLP2, PATATIN-LIKE PROTEIN 2. (1) Refers to results from Guiboileau *et al*. (2013). ER, endosplasmic reticulum.

Among phospholipids, the PE, PI and PA molecular species significantly accumulated in *atg5* mutants, while PS and PG levels decreased. PE is essential for ATG8 conjugation and autophagosome formation. The PE36:4 and PE36:5 forms were more abundant in *atg5*, suggesting they could be the molecular PE species involved in ATG8 lipidation (Gomez *et al.*, 2018). Phagophore formation, whose assembly is controlled by the ATG1 complex, occurs at specific ER subdomains enriched in PI and PI3P (Nishimura *et al.*, 2017). The increase of PI molecular species in *atg5* may reflect the enrichment of ER in PI/PIP3 domains that cannot be used to form phagophores in *atg5* (Fig. 10). Indeed, the over-abundance of PI molecular species in *atg5* and *atg5/sid2* is exacerbated under the N- and S-limiting conditions under which autophagy is normally stimulated (Fig. 10).

PAs that play a role in plant signaling, like several PIs (Munnik & Testerink, 2009), accumulated in a similar manner as PIs in *atg5*. PA accumulation suggests that cell signaling in response to stress could be modified in autophagy mutants (Gomez *et al.*, 2018).

Accumulation of cargoes in autophagy mutants

In addition to the metabolic changes revealed by proteomic data, it is likely that several of the proteins highly accumulated in *atg5* lines could be specific autophagy cargoes that could not be cleared out. We can indeed observe a strong accumulation of NBR1 in *atg5* and *atg5/sid2* irrespective of the growth conditions. Interestingly the peroxisome *S*-nitrosoglutathione reductase (GSNOR), that was recently shown to be targeted by ATG8 in Arabidopsis (Zhan *et al.*, 2018) also accumulated in a SA-independent manner in *atg5* irrespective of the conditions. Similar feature was observed for PEX14 that has been reported as the component of the peroxisomal translocon interacting with LC3-II and needed for pexophagy (van Zutphen *et al.*, 2008; Jiang *et al.*, 2015). Interestingly, all the chloroplast proteins we identified here were less abundant in *atg5* and *atg5/sid2* relative to controls, except the β-amylase 1, the fructose-bisphosphate aldolase 5 and the TPP2 serine protease. Whether these proteins are specific autophagy cargoes remains to be determined. Nevertheless, it is plausible that among the list of proteins overaccumulated in both *atg5* and *atg5/sid2*, reside ATG8-interacting cargoes.

Similarities and differences compared with the maize *atg12* proteome

McLoughlin *et al.* (2018) recently identified a collection of proteins significantly more and less abundant in the *atg12* maize mutants grown with nitrogen or submitted to short nitrogen starvation. Like us, they found that the number of proteins altered under N starvation was higher than that found in plants grown with nitrogen. They also found that the proteins that increased in abundance in *atg12* vs wild-type were associated to peroxisome, ER and cytosol and involved in carbohydrate and FA metabolism, and those that decreased were associated with chloroplast and involved in photosynthesis. Therefore, the proteomic changes observed by McLoughlin *et al.* (2018) and by us in our respective autophagy mutants are highly consistent. Comparing the proteomic changes due to the *atg12* mutations in maize and our list of proteins significantly modified in *atg5* in a SA-independent manner, we indeed find 340 proteins in common, corroborating that similar modifications were due to autophagy defect in maize and in Arabidopsis (Table S12). In agreement with their GO term enrichment that significantly identifies protein families associated to acyl-CoA oxidase, acyl-lipid metabolism and citrate lyase (see Table S12), we can

conclude that the major and common impact of autophagy mutation on metabolic processes in Arabidopsis and maize, is related to lipid metabolism and β-oxidation.

In conclusion, like McLoughlin *et al.* (2018), we enlighten here the strong impact of autophagy defect on lipid metabolism. The presumably accelerated loss of chloroplasts shortens carbon fixation and sugar synthesis on the one hand (Fig. 10; Masclaux-Daubresse *et al.*, 2014; Guiboileau *et al.*, 2013), and provides lipid and protein resources for alternative catabolic routes occurring in the peroxisome, on the other hand (Izumi *et al.*, 2013a; McLoughlin *et al.*, 2018). The increase in several proteases as shown by Havé *et al.* (2018) and the increase of peroxisome enzymes involved in amino acid and lipid catabolism are in line with this. Our data suggest that lipid recycling from endomembranes is impaired in *atg5* mutant, principally impacting ER- and plasma membrane compositions. The formation of cytoplasmic LDs suggested by the increase of PDAT1 at the ER membrane in *atg5* is undetectable possibly due to stimulated β-oxidation. The perturbation of ER proteostasis in *atg5* triggers ER stress.

Therefore, any environmental condition that could amplifies ER stress is believed to amplify metabolic disorders if autophagy machinery is malfunctioning, leading to plant susceptibility. The changes in endomembrane lipid compositions in *atg5* reflected by our results may strongly influence/modify cell-to-cell communication, metabolite and hormone allocation, nutrient transport and long distance signaling in autophagy mutants. Such disorders could explain the defects of autophagy mutants in plant immunity and nutrient allocation.

Acknowledgements

Authors thank the proteomic platform PAPSSO (INRA, Le Moulon, France), and the 'Plateforme Biopuces et Séquençage' of IGBMC (Strasbourg, France) for proteomic and transcriptomic analyses respectively. Thanks to Fabienne Soulay, Joël Talbotec and Philippe Maréchal for taking care of plants. This work was supported the ANR-12-ADAPT-0010-0. The LabEx Saclay Plant Sciences-SPS (ANR-10-LABX-0040-SPS) provided support for IJPB. JL was supported by AgreenSkills international programme for mobility with the support of the AgreenSkills+ fellowship programme which has received funding from the EU's Seventh Framework Program under agreement no. FRP7-609398 (AgreenSkill+ contract). MH was supported by ANR-12-ADAPT-0010-0.

Author contributions

MH, TB and GC performed proteomic experiments under the supervision of LR and MZ. Lipid analyses were performed by FT and J-LC, JL, MH and FC contributed to statistical analyses. JL performed bioinformatic analyses. CM-D and J-LC contributed to the data mining. CM-D supervised the entire work and wrote the manuscript with the help of J-LC. MH and JL contributed equally to this work.

ORCID

Thierry Balliau https://orcid.org/0000-0002-8172-1605
Jean-Luc Cacas https://orcid.org/0000-0002-8961-4505
Fabien Chardon https://orcid.org/0000-0001-7909-3884
Marien Havé https://orcid.org/0000-0002-2234-7043
Jie Luo https://orcid.org/0000-0003-1495-8239
Céline Masclaux-Daubresse https://orcid.org/0000-0003-0719-9350
Loic Rajjou https://orcid.org/0000-0001-9739-1041
Michel Zivy https://orcid.org/0000-0002-9814-3792

References

Avin-Wittenberg T, Bajdzienko K, Wittenberg G, Alseekh S, Tohge T, Bock R, Giavalisco P, Fernie AR. 2015. Global analysis of the role of autophagy in cellular metabolism and energy homeostasis in *Arabidopsis* seedlings under carbon starvation. *Plant Cell* **27**: 306–322.

Balliau T, Blein-Nicolas M, Zivy M. 2018. Evaluation of optimized tube-gel methods of sample preparation for large-scale plant proteomics. *Proteomes* **6**: 6.

Bao Y, Pu YT, Yu X, Gregory BD, Srivastava R, Howell SH, Bassham DC. 2018. IRE1B degrades RNAs encoding proteins that interfere with the induction of autophagy by ER stress in *Arabidopsis thaliana*. *Autophagy* **14**: 1562–1573.

Benjamini Y, Hochberg Y. 1995. Controlling the false discovery rate – a practical and powerful approach to multiple testing. *Journal of the Royal Statistical Society Series B-Methodological* **57**: 289–300.

Bernales S, McDonald KL, Walter P. 2006. Autophagy counterbalances endoplasmic reticulum expansion during the unfolded protein response. *PLoS Biology* **4**: 2311–2324.

Boyle NR, Page MD, Liu BS, Blaby IK, Casero D, Kropat J, Cokus SJ, Hong-Hermesdorf A, Shaw J, Karpowicz SJ *et al.* 2012. Three acyltransferases and nitrogen-responsive regulator are implicated in nitrogen starvation-induced triacylglycerol accumulation in *Chlamydomonas*. *Journal of Biological Chemistry* **287**: 15811–15825.

Cacas J-L. 2015. Out for a walk along the secretory pathway during programmed cell death. In: Gunawardena AH, McCabe P, eds. *Plant programmed cell death*. Powell, WY, USA: Springer. Chapter 6, 123–161.

Cacas JL, Bure C, Grosjean K, Gerbeau-Pissot P, Lherminier J, Rombouts Y, Maes E, Bossard C, Gronnier J, Furt F *et al.* 2016. Revisiting plant plasma membrane lipids in tobacco: a focus on sphingolipids. *Plant Physiology* **170**: 367–384.

Cai Y, Arikkath J, Yang L, Guo ML, Periyasamy P, Buch S. 2016. Interplay of endoplasmic reticulum stress and autophagy in neurodegenerative disorders. *Autophagy* **12**: 225–244.

Dewdney J, Reuber TL, Wildermuth MC, Devoto A, Cui JP, Stutius LM, Drummond EP, Ausubel FM. 2000. Three unique mutants of *Arabidopsis* identify *eds* loci required for limiting growth of a biotrophic fungal pathogen. *The Plant Journal* **24**: 205–218.

Ding WX, Ni HM, Gao WT, Hou YF, Melan MA, Chen XY, Stolz DB, Shao ZM, Yin XM. 2007. Differential effects of endoplasmic reticulum stress-induced autophagy on cell survival. *Journal of Biological Chemistry* **282**: 4702–4710.

Gomez RE, Joubes J, Valentin N, Batoko H, Satiat-Jeunemaitre B, Bernard A. 2018. Lipids in membrane dynamics during autophagy in plants. *Journal of Experimental Botany* **69**: 1287–1299.

Guiboileau A, Avila-Ospina L, Yoshimoto K, Soulay F, Azzopardi M, Marmagne A, Lothier J, Masclaux-Daubresse C. 2013. Physiological and metabolic consequences of autophagy deficiency for the management of nitrogen and protein resources in Arabidopsis leaves depending on nitrate availability. *New Phytologist* **199**: 683–694.

Guiboileau A, Yoshimoto K, Soulay F, Bataillé M, Avice J, Masclaux-Daubresse C. 2012. Autophagy machinery controls nitrogen remobilization at the whole-

plant level under both limiting and ample nitrate conditions in *Arabidopsis*. *New Phytologist* **194**: 732–740.

Havé M, Balliau T, Cottyn-Boitte B, Derond E, Cueff G, Soulay F, Lornac A, Reichman P, Dissmeyer N, Avice J-C *et al.* 2018. Increase of proteasome and papain-like cysteine protease activities in autophagy mutants: backup compensatory effect or pro cell-death effect? *Journal of Experimental Botany* **69**: 1369–1385.

Hildebrandt TM, Nesi AN, Araujo WL, Braun HP. 2015. Amino acid catabolism in plants. *Molecular Plant* **8**: 1563–1579.

Howell SH 2013. Endoplasmic reticulum stress responses in plants. *Annual Review of Plant Biology* **64**: 477–499.

Izumi M, Hidema J, Ishida H. 2013a. Deficiency of autophagy leads to significant changes of metabolic profiles in *Arabidopsis*. *Plant Signaling & Behavior* **8**: e25023.

Izumi M, Hidema J, Makino A, Ishida H. 2013b. Autophagy contributes to nighttime energy availability for growth in *Arabidopsis*. *Plant Physiology* **161**: 1682–1693.

Jiang L, Hara-Kuge S, Yamashita S, Fujiki Y. 2015. Peroxin Pex14p is the key component for coordinated autophagic degradation of mammalian peroxisomes by direct binding to LC3-II. *Genes to Cells* **20**: 36–49.

Kouroku Y, Fujita E, Tanida I, Ueno T, Isoai A, Kumagai H, Ogawa S, Kaufman RJ, Kominami E, Momoi T. 2007. ER stress (PERK/eIF2 alpha phosphorylation) mediates the polyglutamine-induced LC3 conversion, an essential step for autophagy formation. *Cell Death and Differentiation* **14**: 230–239.

Kurusu T, Koyano T, Hanamata S, Kubo T, Noguchi Y, Yagi C, Nagata N, Yamamoto T, Ohnishi T, Okazaki Y *et al.* 2014. *OsATG7* is required for autophagy-dependent lipid metabolism in rice postmeiotic anther development. *Autophagy* **10**: 878–888.

La Camera S, Balague C, Gobel C, Geoffroy P, Legrand M, Feussner I, Roby D, Heitz T. 2009. The *Arabidopsis* Patatin-Like Protein 2 (PLP2) plays an essential role in cell death execution and differentially affects biosynthesis of oxylipins and resistance to pathogens. *Molecular Plant–Microbe Interactions* **22**: 469–481.

La Camera S, Geoffroy P, Samaha H, Ndiaye A, Rahim G, Legrand M, Heitz T. 2005. A pathogen-inducible patatin-like lipid acyl hydrolase facilitates fungal and bacterial host colonization in *Arabidopsis*. *The Plant Journal* **44**: 810–825.

Le Bars R, Marion J, Le Borgne R, Satiat-Jeunemaitre B, Bianchi MW. 2014. ATG5 defines a phagophore domain connected to the endoplasmic reticulum during autophagosome formation in plants. *Nature Communications* **5**: 4121.

Li YH, Beisson F, Pollard M, Ohlrogge J. 2006. Oil content of *Arabidopsis* seeds: the influence of seed anatomy, light and plant-to-plant variation. *Phytochemistry* **67**: 904–915.

Liu F, Marshall RS, Li F. 2018. Understanding and exploiting the roles of autophagy in plants through multi-omics approaches. *Plant Science* **274**: 146–152.

Liu Y, Bassham DC. 2012. Autophagy: pathways for self-eating in plant cells. *Annual Review of Plant Biology* **63**: 215–237.

Liu Y, Burgos JS, Deng Y, Srivastava R, Howell SH, Bassham DC. 2012. Degradation of the endoplasmic reticulum by autophagy during endoplasmic reticulum stress in *Arabidopsis*. *Plant Cell* **24**: 4635–4651.

Luo WJ, Brouwer C. 2013. Pathview: an R/Bioconductor package for pathway-based data integration and visualization. *Bioinformatics* **29**: 1830–1831.

Lyutvinskiy Y, Yang HQ, Rutishauser D, Zubarev RA. 2013. In silico instrumental response correction improves precision of label-free proteomics and accuracy of proteomics-based predictive models. *Molecular & Cellular Proteomics* **12**: 2324–2331.

Masclaux-Daubresse C, Chen Q, Havé M. 2017. Regulation of nutrient recycling via autophagy. *Current Opinion in Plant Biology* **39**: 8–17.

Masclaux-Daubresse C, Clément G, Anne P, Routaboul J, Guiboileau A, Soulay F, Shirasu K, Yoshimoto K. 2014. Stitching together the multiple dimensions of autophagy using metabolomic and transcriptomic analyses reveals new impacts of autophagy defects on metabolism, development and plant response to environment. *Plant Cell* **26**: 1857–1877.

McLoughlin F, Augustine RC, Marshall RS, Li FQ, Kirkpatrick LD, Otegui MS, Vierstra RD. 2018. Maize multi-omics reveal roles for autophagic recycling in proteome remodelling and lipid turnover. *Nature Plants* **4**: 1056–1070.

Minina EA, Moschou PN, Vetukuri RR, Sanchez-Vera V, Cardoso C, Liu QS, Elander PH, Dalman K, Beganovic M, Yilmaz JL *et al.* 2018. Transcriptional stimulation of rate-limiting components of the autophagic pathway improves plant fitness. *Journal of Experimental Botany* **69**: 1415–1432.

Mueller SP, Unger M, Guender L, Fekete A, Mueller MJ. 2017. Phospholipid: diacylglycerol acyltransferase-mediated triacylglycerol synthesis augments basal thermotolerance. *Plant Physiology* **175**: 486–497.

Munch D, Rodriguez E, Bressendorff S, Park OK, Hofius D, Petersen M. 2014. Autophagy deficiency leads to accumulation of ubiquitinated proteins, ER stress, and cell death in *Arabidopsis*. *Autophagy* **10**: 1579–1587.

Munnik T, Testerink C. 2009. Plant phospholipid signaling: 'in a nutshell'. *Journal of Lipid Research* **50**: S260–S265.

Nishimura T, Tamura N, Kono N, Shimanaka Y, Arai H, Yamamoto H, Mizushima N. 2017. Autophagosome formation is initiated at phosphatidylinositol synthase-enriched ER subdomains. *EMBO Journal* **36**: 1719–1735.

Ogata M, Hino SI, Saito A, Morikawa K, Kondo S, Kanemoto S, Murakami T, Taniguchi M, Tanii I, Yoshinaga K *et al.* 2006. Autophagy is activated for cell survival after endoplasmic reticulum stress. *Molecular and Cellular Biology* **26**: 9220–9231.

Pottier M, Dumont J, Masclaux-Daubresse C, Thomine S. 2019. Autophagy is essential for optimal translocation of iron to seeds in *Arabidopsis*. *Journal of Experimental Botany* **70**: 859–869.

Rashid HO, Yadav RK, Kim HR, Chae HJ. 2015. ER stress: autophagy induction, inhibition and selection. *Autophagy* **11**: 1956–1977.

Rottet S, Besagni C, Kessler F. 2015. The role of plastoglobules in thylakoid lipid remodeling during plant development. *Biochimica Et Biophysica Acta-Bioenergetics* **1847**: 889–899.

Shibata M, Oikawa K, Yoshimoto K, Kondo M, Mano S, Yamada K, Hayashi M, Sakamoto W, Ohsumi Y, Nishimura M. 2013. Highly oxidized peroxisomes are selectively degraded via autophagy in *Arabidopsis*. *Plant Cell* **25**: 4967–4983.

Spitzer M, Wildenhain J, Rappsilber J, Tyers M. 2014. BoxPlotR: a web tool for generation of box plots. *Nature Methods* **11**: 121–122.

Sturn A, Quackenbush J, Trajanoski Z. 2002. Genesis: cluster analysis of microarray data. *Bioinformatics* **18**: 207–208.

Tellier F, Maia-Grondard A, Schmitz-Afonso I, Faure JD. 2014. Comparative plant sphingolipidomic reveals specific lipids in seeds and oil. *Phytochemistry* **103**: 50–58.

Tjellstrom H, Strawsine M, Ohlrogge JB. 2015. Tracking synthesis and turnover of triacylglycerol in leaves. *Journal of Experimental Botany* **66**: 1453–1461.

Yang X, Bassham DC. 2015. New insight into the mechanism and function of autophagy in plant cells. *International Review of Cell and Molecular Biology* **320**: 1–40.

Yang XC, Srivastava R, Howell SH, Bassham DC. 2016. Activation of autophagy by unfolded proteins during endoplasmic reticulum stress. *The Plant Journal* **85**: 83–95.

Yorimitsu T, Nair U, Yang ZF, Klionsky DJ. 2006. Endoplasmic reticulum stress triggers autophagy. *Journal of Biological Chemistry* **281**: 30299–30304.

Yoshimoto K, Ishida H, Wada S, Ohsumi Y, Shirasu K. 2009. The role of plant autophagy in nutrient starvation and aging. *Autophagy* **5**: 904.

Yu GC, Wang LG, Han YY, He QY. 2012. clusterProfiler: an R package for comparing biological themes among gene clusters. *Omics-a Journal of Integrative Biology* **16**: 284–287.

Zechner R, Madeo F, Kratky D. 2017. Cytosolic lipolysis and lipophagy: two sides of the same coin. *Nature Reviews Molecular Cell Biology* **18**: 671–684.

Zhan N, Wang C, Chen LC, Yang HJ, Feng J, Gong XQ, Ren B, Wu R, Mu JY, Li YS *et al.* 2018. S-Nitrosylation targets GSNO reductase for selective autophagy during hypoxia responses in plants. *Molecular Cell* **71**: 142–154.

Zientara-Rytter K, Subramani S. 2016. Autophagic degradation of peroxisomes in mammals. *Biochemical Society Transactions* **44**: 431–440.

van Zutphen T, Veenhuis M, van der Klei IJ. 2008. Pex14 is the sole component of the peroxisomal translocon that is required for pexophagy. *Autophagy* **4**: 63–66.

Supporting Information

Additional Supporting Information may be found online in the Supporting Information section at the end of the article.

Fig. S1 Partition of the predicted cellular localisation of the significantly differentially upregulated or downregulated proteins in a SA-independent manner under Ctr, low-N and low-S conditions.

Fig. S2 Functional categories and predicted localisations of the CL proteins.

Fig. S3 Protein changes in the ribosomal proteins of autophagy mutants.

Fig. S4 Protein changes in the pentose phosphate, the glycolysis and the TCA pathways of autophagy mutants.

Fig. S5 Changes in proteins related to amino acid metabolism in autophagy mutants.

Fig. S6 Changes in the total fatty acid (FA) profiles in Col, sid2, *atg5*, *atg5/sid2*.

Fig. S7 Phospholipids composition in Col, *atg5*, *sid2*, *atg5/sid2*.

Fig. S8 Sphingolipid composition in Col, *atg5*, *sid2*, *atg5/sid2*.

Table S1 MRM methods for lipids analysis. The transition (precursor ion/product ion) and the elution time are given for each lipid analysed.

Table S2 KEGG and TAIR10 GO terms of cluster 1.

Table S3 KEGG and TAIR10 GO terms of cluster 2.

Table S4 KEGG and TAIR10 GO terms of cluster 3.

Table S5 KEGG and TAIR10 GO terms of cluster 4.

Table S6 ANOVA and Tukey tests performed to identify protein abundances significantly modified in *atg5* vs Col and *atg5/sid2* vs *sid2*.

Table S7 List of the proteins significantly more or less abundant in *atg5*-deficient plants, in a SA-independent manner and in at least one of the growth conditions.

Table S8 Function of the proteins significantly more or less abundant in *atg5*-deficient plants in an SA-independent manner and in all the three growth conditions.

Table S9 VIRTUALPLANT analysis of the protein lists exclusively modified under Ctr, low-N or low-S conditions.

Table S10 List of the amino acid catabolic enzymes significantly more or less abundant in *atg5* deficient plants, in an SA-independent manner and in at least one of the growth conditions.

Table S11 Phospholipid, galactolipid and sphingolipid concentrations in Col, *atg5*, *sid2*, *atg5/sid2* plants grown in control, low nitrate or low sulfur conditions.

Table S12 List of the Arabidopsis proteins presenting with their maize homologues significant changes in their abundance in both Arabidopsis and maize autophagy mutants.